Investigation of melting point, Debye frequency and temperature of iron at high pressure

Nguyen Ba Duc, Ho Khac Hieu, Pham Thi Minh Hanh, Tran Thi Hai, Nguyen Viet Tuyen, and Tran Thi Ha

THE EUROPEAN
PHYSICAL JOURNAL B

Regular Article

Investigation of melting point, Debye frequency and temperature of iron at high pressure

Nguyen Ba Duc[1], Ho Khac Hieu[2,3], Pham Thi Minh Hanh[4], Tran Thi Hai[5], Nguyen Viet Tuyen[6], and Tran Thi Ha[7,8,a]

[1] Tan Trao University, Km 6, Yen Son, Tuyen Quang 301910, Vietnam
[2] Institute of Research and Development, Duy Tan University, 03 Quang Trung, Hai Chau, Da Nang 550000, Vietnam
[3] Faculty of Natural Sciences, Duy Tan University, 03 Quang Trung, Hai Chau, Da Nang 550000, Vietnam
[4] Hanoi Pedagogical University No2, Nguyen Van Linh, Vinh Phuc 15900, Vietnam
[5] Hong Duc University, 565 Quang Trung, Dong Ve, Thanh Hoa 441430, Vietnam
[6] VNU University of Science, 334 Nguyen Trai, Thanh Xuan, Ha Noi 120000, Vietnam
[7] Laboratory of Advanced Materials Chemistry, Advanced Institute of Materials Science, Ton Duc Thang University, Ho Chi Minh City 758307, Vietnam
[8] Faculty of Applied Sciences, Ton Duc Thang University, Ho Chi Minh City 758307, Vietnam

Abstract. The Debye model has been developed to investigate the pressure effects on melting point, Debye frequency and Debye temperature of iron metal. The analytical expressions of these thermodynamic quantities have been derived as functions of crystal volume compressibility. The pressure dependence of them is studied based on the well-established equation-of-state which includes the contributions of the anharmonic and electronic thermal pressures. We performed numerical calculations for iron up to pressure 350 GPa and compared with experimental data when possible. Our results show that the Debye frequency and Debye temperature increase rapidly with compression, and beyond 150 GPa they behave like linear functions of pressure. From the pressure-dependent melting point of iron, we deduce the temperatures of the Earth's inner-outer core boundary (ICB) and core-mantle boundary (CMB). The temperatures of the Earth's ICB and CMB are predicted lower than 5540($\pm$170) K and about 4060 K, respectively.

1 Introduction

Investigation of thermodynamic properties of iron at high pressure is a subject attracting the interest of many scientists in planetary science, geophysics and nuclear physics. This comes from a fact that iron is a main component in the Earth's core in which it combines with a small amount of light elements such as Si, C, H, O,... Furthermore, the temperature of Earth's inner-outer core boundary (ICB) is proposed to be closed to the melting point of iron at pressure of 330 GPa. Hence, the high-pressure thermo-mechanical properties of iron are of primarily important information to explain geochemical observations and seismic data. Therefore, the understanding of physical properties of iron as well as its alloys at extreme conditions permits us to model the dynamic properties, the composition, the evolution process, the structure and the dynamo of the Earth. Numerous attempts were performed to estimate the physical properties of iron and iron-based alloys

at extreme pressure. Theoretically, the structure and thermodynamic properties of iron at Earth's core conditions have been studied by first-principles calculations [1,2], molecular dynamics simulations coupled with ab initio calculations [3,4] and the thermodynamic integration scheme [5,6]. On the experimental side, along with remarkable developments of high-pressure techniques, researchers could design experiments up to hundreds of gigapascals such as laser-heated diamond-anvil cell (DAC) [7] and shock-wave experiments [8].

The Debye frequency and Debye temperature are two important physical quantities proposed in within view of the Debye model [9]. The Debye temperature could be used to classify the high and low temperature regions on the investigation of thermodynamic properties of solids. By measuring the change of intensity of X-ray diffraction (XRD) lines under pressure, Anderson et al. yielded information of mean square displacement of hexagonal close-packed iron as a function of volume compression. The value of Debye temperature was then determined over a large compression range corresponding to the Earth's

a e-mail: tranthiha@tdtu.edu.vn

inner-core pressure (up to 359.50 GPa) from the measured intensity of the diffraction lines [10].

Regarding the melting problem, the melting point of materials at high pressure has been measured by various techniques such as XRD [11–13], X-ray absorption spectroscopy (XAS) [14], synchrotron Mössbauer spectroscopy [15], and theoretical methods [16–18]. Notwithstanding, the estimation of high-pressure melting temperature of iron is still a matter of debate among different studies. For instance, from the laser-heated DAC experiment results, Boehler extrapolated the melting point of iron to 330 GPa corresponding to the pressure at ICB to be 4850(±200) K [19]. Using synchrotron-based fast XRD as a primary melting diagnostic, Anzellini et al. obtained the melting temperature of iron to be 6230 ± 500 K at 330 GPa by extrapolating their results from 200 GPa [15]. This estimation of Anzellini et al. is reasonably consistent with shock compression data [8] and theoretical predictions [20]. Meanwhile the two recent works based on XAS [21] and synchrotron Mössbauer spectroscopy [22] showed that melting curves of iron were significantly lower than the calculations of Anzellini et al. [15].

In present study, the correlated Debye model is applied to investigate the Debye frequency and temperature, and melting temperature of iron under compression. Numerical calculations are performed up to pressure 350 GPa corresponding to the Earth's inner core conditions and compared with those of previous works when possible. From the derived melting point of iron, we estimate the temperatures of the Earth's ICB and the core-mantle boundary (CMB).

2 Methodology

2.1 Debye frequency and temperature

Considering a crystal with N atoms, the Debye model assumes a homogeneous system with a constant speed of sound v and a linear dispersion relation $\omega = v.k$ (where k is the wavenumber). The maximum of phonon frequency is called the Debye frequency ω_D. The Debye temperature is calculated through its relation to Debye frequency as $\theta_D = \hbar\omega_D/k_B$ (where $\hbar$ is the reduced Planck constant and k_B is the Boltzmann constant), above which all modes start to be excited and below which modes begin to be "frozen out" [9]. In this Debye model, the effect of compression on the Debye frequency ω_D is considered through a physical quantity, the Grüneisen parameter γ_G, defined as

$$\gamma_G = -\frac{\partial \ln \omega_D}{\partial \ln V} = -\frac{\partial \ln \theta_D}{\partial \ln V}, \quad (1)$$

where V is the volume of crystal.

Previous works [23–25] showed that at low pressure, the Grüneisen parameter could be assumed as a constant but it reduces gradually when pressure increases. On the determination of compression effect on Grüneisen parameter, Graf et al. assumed the power-law form for the Grüneisen parameter as $\gamma_G = \gamma_0\zeta^p$, where $p > 0$ is the material constant, γ_0 and V_0 are the Grüneisen

parameter and volume of crystal at ambient conditions, respectively, and ζ is the volume compression ratio $\zeta = V/V_0$ [26,27]. However, this assumption does not describe well the compression effects on the Grüneisen parameter of materials. The calculations of Graf et al. showed that the output results of Grüneisen parameter depend strongly on the chosen approximations (based on the Debye-Waller factor or the bulk modulus) and the pressure range [26]. In particular, they found that the Grüneisen parameter calculated with approximation based on the thermal mean-square displacement is more accurate than the one using the bulk modulus approximation at low compression, and vice versa. Recently, Burakovsky et al. proposed an analytic three-parameter model of the Grüneisen parameter of solid at all densities as [28,29] $\gamma_G = 1/2 + \gamma_1\zeta^{1/3} + \gamma_2\zeta^q$, where $\gamma_1, \gamma_2, q = $ const, $q > 1$. This expression is derived in within the Thomas–Fermi approximation by means of the consideration of low- and ultra-high-pressure limit conditions. However, the result from fitting experimental measurements of iron [10] with this model is still not really good, especially at ambient and high pressure regions [30]. In this paper, another well-described form of Grüneisen parameter following the Al'tshuler et al. proposition [31] has been chosen as follows [32]

$$\gamma_G = \gamma_\infty + (\gamma_0 - \gamma_\infty)\zeta^\beta, \quad \text{with} \quad \beta = \frac{\gamma_0}{\gamma_0 - \gamma_\infty}, \quad (2)$$

where γ_0 and γ_∞ are, respectively, the values of Grüneisen parameter γ_G at ambient conditions and infinite compression. This form of the Grüneisen parameter could be seen as an expansion of the power-law suggested by Graf et al. Using previous experimental shock-wave data up to 200 GPa (before any possible structural phase transition [33] and melting [8]), together with their measurements at ambient conditions, Dewaele et al. [32] estimated the values of γ_0 and γ_∞ for iron.

By substituting equations (2) into (1) and taking the integral, we find out the Debye frequency and Debye temperature as functions of volume compression $\zeta = V/V_0$, respectively, as

$$\omega_D(\zeta) = \omega_0\zeta^{-\gamma_\infty} \exp\left\{-\frac{\gamma_0}{\beta^2}(\zeta^\beta - 1)\right\}, \quad (3)$$

and

$$\theta_D(\zeta) = \theta_0\zeta^{-\gamma_\infty} \exp\left\{-\frac{\gamma_0}{\beta^2}(\zeta^\beta - 1)\right\}, \quad (4)$$

where ω_0 and $\theta_0 = k_B\omega_0/\hbar$ are, correspondingly, the values of Debye frequency and temperature of iron at ambient conditions. These values can be measured from experiments or determined from the correlated Debye model [34].

2.2 Melting temperature

On the investigation of the melting point of materials, the Lindemann's melting criterion is one of the most

well-known theories that has been widely used for the melting instability [35,36]. This criterion was proposed as follows [37]: a solid material starts melting when the ratio of the square-root of atomic mean-square displacement to the nearest-neighbor distance between two intermediate atoms attains a threshold value. Applying this Lindemann's proposition, the pressure-dependent melting points of many metals have been derived empirically in a number of literatures before [35,38,39]. Based on the ideas of the classical mean field potential approach, the Lindemann's criterion has been re-written in a more general form as [40]

$$T_m = \text{const} \times V^{\frac{2}{3}}.\theta_D^2. \qquad (5)$$

By taking the natural logarithm and volume derivatives of both sides of equation (5), we obtain the following equation

$$\frac{\partial \ln(T_m)}{\partial V} = \frac{2}{V}\left(\frac{1}{3} - \gamma_G\right), \qquad (6)$$

where the Grüneisen parameter γ_G is defined as equation (1) in Debye model.

Substituting equation (2) of the volume-dependent Grüneisen parameter formula into equation (6) and taking integral, we find out the expression of melting point T_m of iron as a function of volume compression ζ as

$$T_m(\zeta) = T_0\zeta^{2(1/3-\gamma_\infty)} \exp\left\{\frac{2(\gamma_0 - \gamma_\infty)}{\beta}\left(1 - \zeta^\beta\right)\right\}, \quad (7)$$

where T_0 is the melting point of iron at ambient conditions.

2.3 Equation-of-state of iron

In order to study the pressure effects on these above thermodynamic quantities of iron (Debye frequency and temperature, and melting temperature), we need an accurate high-pressure and high-temperature P-V-T relation (or equation-of-state - EOS). Most frequently EOSs for the investigation of high-pressure thermodynamic properties and pressure-induced phase transitions of materials are Birch-Murnaghan EOS, Vinet EOS, Holzapfel EOS,... In this work, we choose the EOS derived by Dewaele et al. [32]. Accordingly, the total pressure $P(V,T)$ is expressed as the sum of cold (isothermal) pressure and temperature-dependent (thermal) presssure

$$P(V,T) = P_V(V, 300\,\text{K}) + [P_{\text{TH}}(V,T) - P_{\text{TH}}(V, 300\,\text{K})], \qquad (8)$$

where $P_V(V, 300\,\text{K})$ is the isothermal pressure at temperature $300\,\text{K}$ and $P_{\text{TH}}(V,T)$ is the temperature-dependent pressure.

In this paper, $P_V(V, 300\,\text{K})$ and $P_{\text{TH}}(V,T)$ are expressed using the fitted Vinet EOS [41] and the formalism derived by Dorogokupets and Oganov [42,43] by

equations (9) and (10), respectively, as

$$P_V(V, 300\,\text{K}) = 3B_0\zeta^{-2/3}\left(1 - \zeta^{1/3}\right) \qquad (9)$$
$$\times \exp\left[\frac{3}{2}(B_0' - 1)\left(1 - \zeta^{1/3}\right)\right],$$

$$P_{\text{TH}}(V,T) = \frac{9R\gamma_G}{V}\left[\frac{\theta_D}{8} + T\left(\frac{T}{\theta_D}\right)^3\int_0^{\theta_D/T}\frac{y^3 dy}{e^y - 1}\right]$$
$$+ \frac{3R}{2V}(b_0 m\zeta^m + e_0 n\zeta^n)T^2, \qquad (10)$$

where B_0 and B_0' are the isothermal bulk modulus and the first-pressure derivative of isothermal bulk modulus, respectively; R denotes the gas constant. The first term of the right-hand side of equation (10) represents the main part of P_{TH}, which is the quasiharmonic Debye thermal pressure [41]. The second term includes the contributions of the anharmonic and electronic thermal pressure [44]. Their parameters b_0, e_0, m and n have been derived for iron by fitting first-principles anharmonic and electronic thermal pressures as [32] $b_0 = 3.7 \times 10^{-5}$ K^{-1}, $e_0 = 1.95 \times 10^{-4}$ K^{-1}, $m = 1.87$ and $n = 1.339$. With the aid of equations (8)–(10) we can numerically determine the Debye frequency and Debye temperature, and melting temperature of iron as functions of pressure P.

3 Result and discussion

In this section, the numerical calculations are performed for iron up to 350 GPa. For this purpose, the Debye temperature θ_{0D} at ambient conditions is fixed as 417 K, the isothermal bulk modulus B_0 and its first-pressure derivative B_0' are, respectively, as 163.4 GPa and 5.38 [32]. By substituting our fitted values of γ_0 and γ_∞ of iron into equations (3) and (4) with Debye temperature $\theta_0 = 417$ K and Debye frequency $\omega_0 = k_B\theta_0/\hbar = 5.46 \times 10^{13}$ Hz at ambient conditions, we get the ω_D and θ_D of iron as functions of volume compression ζ. With the aid of EOS equation (8), the pressure dependence of the Debye frequency and temperature can be investigated. This combination of Grüneisen parameter following the Al'tshuler et al. proposition and Vinet EOS will be referred to as AV model. We show these two pressure-dependent thermodynamic quantities in Figure 1. It is clear from this figure that the Debye frequency and Debye temperature increase robustly with pressure. The rise of the phonon frequency can be explained by the reduction of atomic vibrations amplitudes due to the increasing of compression. Beyond 150 GPa, the slopes of Debye frequency and temperature curves become reducible and they are almost linear proportional to pressure. The initial slope of these curves is about 4.4 K/GPa but from pressure 150 GPa and beyond, the average slope is about 1.2 K/GPa. Furthermore, in Figure 1, we also present the results of Debye temperature and Debye frequency (circle and square symbols) in Anderson et al.' work [10] for comparison. Anderson et al. have extracted these thermodynamic quantities from the
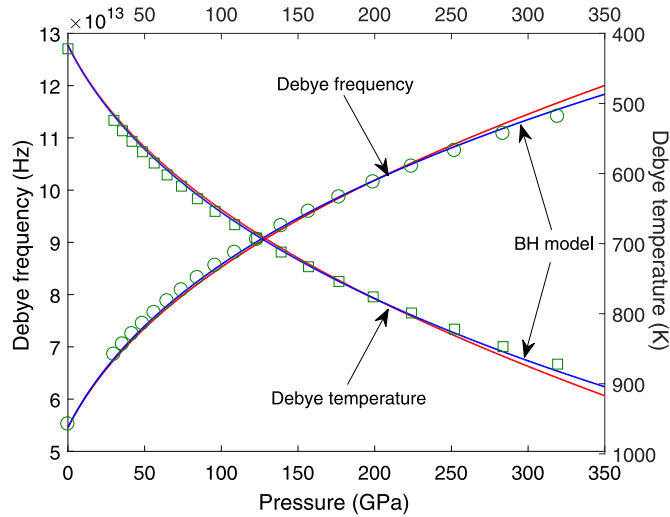
Fig. 1. Pressure dependence of Debye frequency and Debye temperature of iron. Our theoretical curves (red solid & dashed lines (AV model), blue solid & dashed lines (BH model)) are shown along with those deduced from experimental mean-square displacements [10] (green circle and square symbols) for comparison.

Table 1. Melting temperature of iron under pressure at temperature $T = 300$ K.

Pressure (GPa)	Present work (K)		Sinmyo et al. [46] (K)
	$T_0 = 1811$ K	$T_0 = 1608$ K	
97	3580	3180	3030 ± 75
134	4040	3585	3470 ± 85
136	4060	3605	–
151	4230	3760	3610 ± 90
200	4745	4215	–
230	5040	4475	4780 ± 120
257	5290	4700	–
290	5580	5955	5360 ± 140
300	5665	5030	–
330	5920	5260	5500 ± 220
350	6080	5400	–

atomic mean-square displacements which were obtained by X-ray structural refinement using the Rietveld method on powder diffraction measurements [10]. As it can be observed from Figure 1, our theoretical calculations follow the data of Anderson et al. up to pressure about 300 GPa. At pressure higher than 300 GPa, the calculations of Debye frequency and corresponding Debye temperature are slightly different from those measured by XRD experiments. The overestimation of theoretical Debye temperature (and Debye frequency) comparing to Anderson et al.' work progressively increases with pressure, about 0.5% at 350 GPa.

Now we present the pressure dependence of the melting point T_m of iron metal. Firstly, the melting curve of iron is plotted with the ambient melting temperature $T_0 = 1811$ K derived from experiments. Figure 2 shows our calculated melting curve in conjunction with the selected recent experimental static-compression, shock-compression, XAS and synchrotron Mössbauer spectroscopy measurements up to 350 GPa, higher than the pressure of the Earth ICB. On the theoretical side, as it can be clearly observed from Figure 2, present theoretical melting curve of iron goes along with previous predictions proposed by Alfè [20] and Anzellini et al. [15]. Being compared to experiments, our calculated melting points are reasonable in keeping with those of previous measurements in two pressure ranges $P < 70$ GPa and $P > 230$ GPa. Especially, our melting line of iron follows well the recent static compression experiments measured by internal-resistance-heated DAC up to 100 GPa [45], and up to 290 GPa [46]. However, the deviation between theory and experiments can also be observed in the pressure range $(70 < P < 230$ GPa). Anzellini et al. explained the underestimation of melting temperature in measurements is due to the fast recrystallization process instead

of melting. The melting points of iron in our calculations at some selected pressures are shown in Table 1.

It should be noted that light elements (Si, O, S, C, H,...) included in the liquid outer core will depress melting temperature of iron alloys [54] then the upper limit for the temperature at the boundary of Earth's core and outer core can be approximated from the melting point of iron at pressure 330 GPa [22,46,55]. By assuming the linear depression of liquidus temperature with increasing the concentration of single light element in iron alloys [56], Sinmyo et al. derived the temperature depression induced by the theoretically predicted maximum concentrations 7 wt% Si, 5 wt% O, 9 wt% S, 4 wt% C [57], and 1.0 wt% H [57,58] in outer core density are 210($\pm$210) K by Si, 450($\pm$150) K by O and H, 1350($\pm$810) K by S, and 1880($\pm$1360) K by C [46], respectively. They found that the minimum temperature depression is attained when the core contains 7 wt% Si. However, because the eutectic liquid in the Fe-FeSi binary includes less than 2 wt% Si and liquid Fe with greater than 2 wt% Si crystallizes CsCl-type Fe–Si alloy [59], Sinmyo et al. also showed that the least depression of the outer core liquidus temperature is 380($\pm$170) K when the system is consisted of 2 wt% Si and 3.6 wt% O (or 0.7 wt% H) [46]. In our calculations, the melting point of iron at 330 GPa is about 5920 K. Consequently, the Earth's ICB should be lower than 5540($\pm$170) K. The present prediction is reasonable in consonance with those of Terasaki et al. (5630 $\pm$ 350 K) [55] and Zhang et al. (5700 $\pm$ 200 K) [22]. It is higher than those of Boehler (5100 K) [19], Laio et al. (5400 K) [60], Sinmyo et al. (5120($\pm$390) K) [46]; and smaller than the values extrapolated by Anzellini et al. (6230 $\pm$ 500 K) [15] and Alfé (6370 $\pm$ 100 K) [20].

Furthermore, at a pressure representative of the CMB (about 136 GPa) [56], the melting point of iron in this work is 4060 K. This result is in good agreement with recent XRD measurements made in the laser-heated DAC, shock-wave experiments and first-principles calculations yielding the melting point for iron at CMB pressure of 4200 K [15]. Then the upper bound for the temperature at CMB is deduced about 3680($\pm$170) K. Our calculation is consistent with the values derived by Sinmyo et al. 3760($\pm$290) K [46], Andrault et al. 3800($\pm$150) K [61]. And it is 300 K smaller than that were measured using
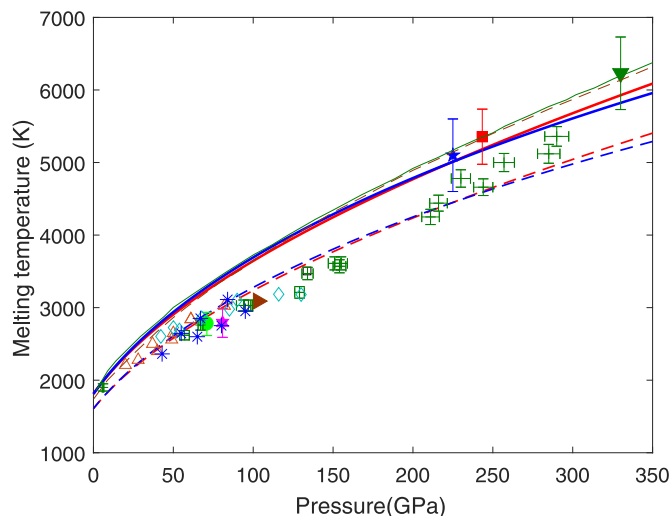
Fig. 2. Melting line of iron under pressure. Our curves (red solid & dashed lines (AV model), blue solid & dashed lines (BH model)) are shown along with those of previous works for comparison. Fast XRD measurements by Anzellini et al. [15] (closed downward pointing triangle and green solid curve); the XAS measurements by Aquilanti et al. [21] (filled right pointing triangle); shock-compressions by Brown and McQueen [47] (filled square), Ahrens et al. [48] (filled circle), and Nguyen and Holmes [8] (filled pentagram); the static-compression XRD experiments by Ma et al. [49] (filled diamond), Shen et al. [50] (filled hexagram), and Boehler et al. [51] (open diamond); synchrotron Mössbauer spectroscopy by Jackson et al. [52] (open upward pointing triangles); static-compression using internal-resistance-heated DAC by Sinmyo et al. [46] (+ marks) and Basu et al. [45] (∗ marks); and ab initio calculations by Bouchet et al. [53] (brown dashed line).

laser-heated DAC by Pradhan et al. 3970(±150) K [62] and Anzellini et al. (4050 ± 500 K) [15].

It is worth mentioning that the melting curve in this approach shows interesting behavior if we replace the experimental ambient melting temperature of iron by the one extracted from literature [49] $T_0 = 1608$ K. The melting curve (the dashed-line) in this case is in a very good agreement with previous reported melting points up to pressure 330 GPa. For example, the melting temperatures of iron inferred from resistivity measurements at 5 GPa and 9 GPa are, respectively, 1880 K and 1990 K. [63,64]. In our calculations, values of T_m at these pressures are, respectively, 1956 K and 2060 K. At pressure 103 GPa, by XAS technique Aquilanti et al. obtained the melting point of iron in a laser-heated DAC of 3090 K [21]. At 135 GPa, the measurements performed by Ahrens et al. [48] (using shock-compression melting experiments) and Boehler [19] (using laser-heated static-compression experiments) gave the melting points of iron 3400 ± 200 K, 3200 ± 100 K, respectively. Meanwhile, the results in our predictions at pressure 103 GPa and 135 GPa are 3250 K and 3606 K, respectively.

An important question that needs further discussion is about some essential sources which cause the discrepancy in investigation of iron melting point at high pressure.

Firstly, previous works showed that the Lindemann's melting criterion maybe work well for many metals but not for all of them at high pressure [7,39]. One of the reasons is caused by the lack of the consideration of electronic configuration of iron in this criterion [65]. Moreover, this melting approach did not take into account point defects, vacancies, dislocations, grain boundaries, and voids which may make an contribution to the bulk melting transition [36]. Secondly, the anharmonicity contribution of lattice vibrations has been neglected in the harmonic approximation of Debye model. This would underestimate the melting point of iron at high temperature where the thermal lattice vibrations become considerable. Thirdly, the experiments of high-pressure melting temperature have been employed with various melting criteria which may produce the fluctuation of measured values. For instance, in XRD techniques, the appearance of diffuse scattering upon melting and the disappearance of diffraction lines could be caused by the loss of long-range order but not by a change in atomic mobility. Nevertheless, such criteria are not easy to be achieved and reproduced at high pressures as a result of the changes in absorption properties and the recrystallization of sample [52]. Furthermore, in laser-heated DAC experiments, the variation of spatial and temporal temperature of samples is large, especially in the direction parallel to the compression axis. Finally, the highest pressure experimentally generated by the previous works is about 200 GPa. A long extrapolation made by authors to the pressure of Earth's inner core might cause a large uncertainty.

Before making conclusions, it should be noted that in order to verify the validity of the proposed approach, we use another Grüneisen parameter model (e.g. Burakovsky's model [28]) and another EOS (e.g. Holzapfel EOS [66]) to derive pressure-dependent Debye frequency and temperature, and melting temperature of iron. This will be referred to as BH model. The volume-dependent expressions of the Debye frequency ω_D, the Debye temperature θ_D, and melting temperature T_m are then derived, respectively, as

$$\omega_D(\eta) = \omega_{0D}\eta^{-1/2}\exp\left\{3\gamma_1\left(1-\eta^{1/3}\right)+\frac{\gamma_2}{q}\left(1-\eta^p\right)\right\},$$
(11)

$$\theta_D(\eta) = \theta_{0D}\eta^{-1/2}\exp\left\{3\gamma_1\left(1-\eta^{1/3}\right)+\frac{\gamma_2}{q}\left(1-\eta^p\right)\right\},$$
(12)

and

$$T_m = T_0\eta^{-1/3}\exp\left\{6\gamma_1\left(1-\eta^{1/3}\right)+\frac{2\gamma_2}{q}\left(1-\eta^q\right)\right\},$$
(13)

where fitted parameters for iron [30] are $\gamma_1 = -0.1603$, $\gamma_2 = 1.4092$ and $q = 1.0003$.

Numerical calculations for pressure dependence of these above thermodynamic quantities using Holzapfel EOS with AP2 form [66] have also been performed and shown in Figures 1 and 2. As observed from these two figures, the Debye frequency ω_D, the Debye temperature θ_D, and

melting temperature T_m derived using BH model are in good accordance with AV model up to pressure about 230 GPa. Beyond 230 GPa, the discrepancy between two models starts to appear and develops together with the increasing of pressure. It is worth to mention also that the pressure 222 ± 6 GPa may be the boundary in which the hcp-iron completely transforms to bcc-iron phase at temperature 4192 ± 104 K [67].

4 Conclusions

In conclusion, the Debye model has been applied to investigate the pressure dependence of the Debye frequency and temperature, and melting temperature of iron based on the definition of the Grüneisen parameter in the Debye model. We derived the analytical expressions of these thermodynamic quantities as functions of volume compression in within the Debye model. Numerical calculations were performed for iron up to pressure 350 GPa of Earth's inner core. Our work shows that the Debye frequency and Debye temperature increase rapidly with compression, and beyond 150 GPa they behave like linear functions of pressure. From the melting point of iron, we estimate the temperatures of the Earth's inner-outer core boundary and core-mantle boundary. The temperature of the Earth's inner-outer core boundary is predicted lower than $5540(\pm 170)$ K and the temperature of the core-mantle boundary is about 4060 K. The reported results increase the database of high-pressure melting temperature of iron, and can be useful for geophysical investigation.

Author contribution statement

All authors contributed equally to the paper.

References

1. L. Stixrude, Phys. Rev. Lett. **108**, 055505 (2012)
2. M. Pozzo, D. Alfè, Phys. Rev. B **88**, 024111 (2013)
3. L. Burakovsky, N. Burakovsky, M.J. Cawkwell, D.L. Preston, D. Errandonea, S.I. Simak, Phys. Rev. B **94**, 094112 (2016)
4. S. Baty, L. Burakovsky, D. Preston, Crystals **10**, 20 (2020)
5. D. Alfé, Rev. Mineral. Geochem. **71**, 337 (2010)
6. H.K. Hieu, T.T. Hai, N.T. Hong, N.D. Sang, N.V. Tuyen, J. Electron. Mater. **46**, 3702 (2017)
7. D. Errandonea, Phys. Rev. B **87**, 054108 (2013)
8. J.H. Nguyen, N.C. Holmes, Nature **427**, 339 (2004)
9. N.W. Ashcroft, N.D. Mermin, *Solid State Physics*, 1st edn. (Cengage Learning, Boston, 1976)
10. O.L. Anderson, L. Dubrovinsky, S.K. Saxena, T. LeBihan, Geophys. Res. Lett. **28**, 399 (2001)
11. D. Santamaria-Perez, M. Ross, D. Errandonea, G.D. Mukherjee, M. Mezouar, R. Boehler, J. Chem. Phys. **130**, 124509 (2009)
12. D. Errandonea, S.G. MacLeod, L. Burakovsky, D. Santamaria-Perez, J.E. Proctor, H. Cynn, M. Mezouar, Phys. Rev. B **100**, 094111 (2019)
13. S. Anzellini, V. Monteseguro, E. Bandiello, A. Dewaele, L. Burakovsky, D. Errandonea, Sci. Rep. **9**, 13034 (2019)
14. Y. Ping, F. Coppari, D.G. Hicks, B. Yaakobi, D.E. Fratanduono, S. Hamel, J.H. Eggert, J.R. Rygg, R.F. Smith, D.C. Swift et al., Phys. Rev. Lett. **111**, 065501 (2013)
15. S. Anzellini, A. Dewaele, M. Mezouar, P. Loubeyre, G. Morard, Science **340**, 464 (2013)
16. T.T. Hai, H.K. Hieu, VNU Journal of Science: Mathematics - Physics **33**, 1 (2017)
17. H.K. Hieu, N. Viet Tuyen, V.N. Nguyen, B.D. Nguyen, Q.T. Vu, T.H. Tran, Q.K. Doan, Curr. Appl. Phys. **19**, 55 (2019)
18. H.K. Hieu, N.T. Hong, D.Q. Khoa, J. Phys. Soc. Jpn. **88**, 105002 (2019)
19. R. Boehler, Nature **363**, 534 (1993)
20. D. Alfè, Phys. Rev. B **79**, 060101 (2009)
21. G. Aquilanti, A. Trapananti, A. Karandikar, I. Kantor, C. Marini, O. Mathon, S. Pascarelli, R. Boehler, Proc. Natl. Acad. Sci. U.S.A. **112**, 12042 (2015)
22. D. Zhang, J.M. Jackson, J. Zhao, W. Sturhahn, E.E. Alp, M.Y. Hu, T.S. Toellner, C.A. Murphy, V.B. Prakapenka, Earth Planet. Sci. Lett. **447**, 72 (2016)
23. R. Boehler, Phys. Rev. B **27**, 6754 (1983)
24. M. Kumari, N. Dass, Phys. Status Solidi B **133**, 101 (1986)
25. H.K. Hieu, Vacuum **109**, 184 (2014)
26. M.J. Graf, C.W. Greeff, J.C. Boettger, AIP Conf. Proc. **706**, 65 (2004)
27. H.K. Hieu, N.N. Ha, AIP Adv. **3**, 112125 (2013)
28. L. Burakovsky, D.L. Preston, J. Phys. Chem. Solids **65**, 1581 (2004)
29. H.K. Hieu, Vacuum Part A **120**, 13 (2015)
30. H.K. Hieu, T.T. Hai, N.T. Hong, N.D. Sang, N.V. Tuyen, High Pressure Res. **37**, 267 (2017)
31. L.V. Al'tshuler, S.E. Brusnikin, E.A. Kuz'menkov, J. Appl. Mech. Tech. Phys. **28**, 129 (1987)
32. A. Dewaele, P. Loubeyre, F. Occelli, M. Mezouar, P.I. Dorogokupets, M. Torrent, Phys. Rev. Lett. **97**, 215504 (2006)
33. M.J. Brown, Geophys. Res. Lett. **28**, 4339 (2001)
34. E. Sevillano, H. Meuth, J.J. Rehr, Phys. Rev. B **20**, 4908 (1979)
35. L. Burakovsky, D.L. Preston, R.R. Silbar, J. Appl. Phys. **88**, 6294 (2000)
36. D. Errandonea, Physica B **357**, 356 (2005)
37. F. Lindemann, Physik Z. **11**, 609 (1910)
38. D. Errandonea, J. Appl. Phys. **108**, 033517 (2010)
39. H.K. Hieu, J. Appl. Phys. **116**, 163505 (2014)
40. Y. Wang, R. Ahuja, B. Johansson, Phys. Rev. B **65**, 014104 (2001)
41. O.L. Anderson, *Equations of State for Solids in Geophysics and Ceramic Science,* Oxford Monographs on Geology and Geophysics (Oxford University Press, Oxford, 1995)

42. P. Dorogokupets, A. Oganov, Dokl. Earth Sci. **410**, 1091 (2006)

43. P.I. Dorogokupets, A.R. Oganov, Phys. Rev. B **75**, 024115 (2007)

44. D. Alfè, G.D. Price, M.J. Gillan, Phys. Rev. B **64**, 045123 (2001)

45. A. Basu, M.R. Field, D.G. McCulloch, R. Boehler, Geosci. Front. **11**, 565 (2020)

46. R. Sinmyo, K. Hirose, Y. Ohishi, Earth Planet. Sci. Lett. **510**, 45 (2019)

47. J.M. Brown, R.G. McQueen, J. Geophys. Res. Solid Earth **91**, 7485 (1986)

48. T.J. Ahrens, K.G. Holland, G.Q. Chen, Geophys. Res. Lett. **29**, 54 (2002)

49. Y. Ma, M. Somayazulu, G. Shen, H. kwang Mao, J. Shu, R.J. Hemley, Phys. Earth Planet. Inter. **143-144**, 455 (2004)

50. G. Shen, H.k. Mao, R.J. Hemley, T.S. Duffy, M.L. Rivers, Geophys. Res. Lett. **25**, 373 (1998)

51. R. Boehler, D. Santamaria-Perez, D. Errandonea, M. Mezouar, J. Phys.: Conf. Ser. **121**, 022018 (2008)

52. J.M. Jackson, W. Sturhahn, M. Lerche, J. Zhao, T.S. Toellner, E.E. Alp, S.V. Sinogeikin, J.D. Bass, C.A. Murphy, J.K. Wicks, Earth Planet. Sci. Lett. **362**, 143 (2013)

53. J. Bouchet, S. Mazevet, G. Morard, F. Guyot, R. Musella, Phys. Rev. B **87**, 094102 (2013)

54. D. Alfe, M. Gillan, G. Price, Earth Planet. Sci. Lett. **195**, 91 (2002)

55. H. Terasaki, S. Kamada, T. Sakai, E. Ohtani, N. Hirao, Y. Ohishi, Earth Planet. Sci. Lett. **304**, 559 (2011)

56. G. Morard, D. Andrault, D. Antonangeli, Y. Nakajima, A. Auzende, E. Boulard, S. Cervera, A. Clark, O. Lord, J. Siebert et al., Earth Planet. Sci. Lett. **473**, 94 (2017)

57. J. Badro, A.S. Côté, J.P. Brodholt, Proc. Natl. Acad. Sci. U.S.A. **111**, 7542 (2014)

58. K. Umemoto, K. Hirose, Geophys. Res. Lett. **42**, 7513 (2015)

59. H. Ozawa, K. Hirose, K. Yonemitsu, Y. Ohishi, Earth Planet. Sci. Lett. **456**, 47 (2016)

60. A. Laio, S. Bernard, G.L. Chiarotti, S. Scandolo, E. Tosatti, Science **287**, 1027 (2000)

61. D. Andrault, G. Pesce, M.A. Bouhifd, N. Bolfan-Casanova, J.M. Hénot, M. Mezouar, Science **344**, 892 (2014)

62. G.K. Pradhan, G. Fiquet, J. Siebert, A.L. Auzende, G. Morard, D. Antonangeli, G. Garbarino, Earth Planet. Sci. Lett. **431**, 247 (2015)

63. R.E. Silber, R.A. Secco, W. Yong, J.A.H. Littleton, Sci. Rep. **8**, 10758 (2018)

64. I.C. Ezenwa, R.A. Secco, Crystals **9**, 359 (2019)

65. S. Japel, B. Schwager, R. Boehler, M. Ross, Phys. Rev. Lett. **95**, 167801 (2005)

66. W.B. Holzapfel, High Pressure Research **16**, 81 (1998)

67. R. Hrubiak, Y. Meng, G. Shen, arXiv:1804.05109 (2018)